Microporous and Mesoporous Materials 380 (2024) 113314

Contents lists available at ScienceDirect

Microporous and Mesoporous Materials

journal homepage: www.elsevier.com/locate/micromeso

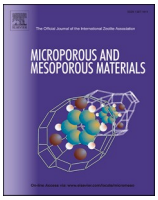

Solid-state microwave assisted batch and flow synthesis, and life cycle assessment, of titanium containing UVM-7 mesoporous silica

Cristina Rodríguez-Carrillo [a], Miriam Benítez [a], Marta González-Fernández [a], Ruth de los Reyes [b], Sonia Murcia [c], Jamal El Haskouri [c], Pedro Amorós [c], Jose V. Ros-Lis [a,*]

[a] REDOLí Research group, Instituto Interuniversitario de Investigación de Reconocimiento Molecular y Desarrollo Tecnológico (IDM), Universitat Politècnica de València, Universitat de València. Doctor Moliner 50, Burjassot, Valencia, 46100, Spain
[b] Microbiotech. S.L. Villamarxant, 46191, Spain
[c] Institut de Ciència Dels Materials (ICMUV), Universitat de València, c/ Catedrático José Beltrán 2, Paterna, Valencia, 46980, Spain

ARTICLE INFO

Keywords:
Microwave-assisted synthesis
Titanium
Mesoporous silica
Flow synthesis
LCA

ABSTRACT

UVM-7 is a bimodal mesoporous silica material that can be prepared in a short time with microwave assisted synthesis (MAS). It is prepared following the atrane route, that allows the synthesis of mixed silicas including other elements with homogeneous distribution. We report herein the preparation of Ti-UVM-7 with using the atrane route in combination with MAS with solid-state generators. The synthesis has been optimized and scaled-up in batch. Also, the flow synthesis has been developed. These materials have not been prepared before using solid-state generators, nor microwave-assisted flow chemistry. The materials have been characterized by XRD, N_2 adsorption-desorption, TEM, EDX, Raman, and Z potential. The materials can be prepared in less than 10 min with a Si/Ti ratio of up to 3.8, and a homogeneous Ti distribution within the UVM-7 silica structure. Scaled-up synthesis produces 33 g of Ti-UVM-7 in 10 min and 12 g h^{-1} in batch and flow synthesis respectively. The optical properties and sun protection factor of the resulting materials were studied. The band gap decreases as titanium concentration increases, reaching 4.1 eV for the highest concentration. Life Cycle Assessment confirms a strong reduction in the impact derived from the scale-up with similar values of approximately 10 points in the single score for the preparation of 1 kg of Ti-UVM-7.

1. Introduction

In recent years, the synthesis of advanced materials has gained significant attention in various scientific fields, owing to their unique properties and potential applications. Mesoporous silica materials such as MCM-41 (hexagonal), MCM-48 (cubic), MCM-50 (lamellar), or the SBA family, have emerged as versatile platforms for catalysis [1], drug delivery [2], sensing [3], and energy storage [4].

Within this family, UVM-7 is a material of special interest. The UVM-7 material was first synthesized at the University of Valencia in 2002 via the atrane route synthesis procedure [5]. It presents a bimodal porous structure formed by intraparticle mesopores (accessible after the removal of the surfactant micelles) and an interparticle textural pore system of large-meso or macropores. It forms a connected network of covalently bonded mesoporous nanoparticles with pseudo-spherical shape, assembled to create a secondary system characterized by large, disorganized textural pores [6]. With a significantly high surface area and a remarkably pore accessibility due to the 3D interconnection of both pore systems, this material stands out as a versatile candidate for a wide range of applications as a support material in catalysis [7], adsorption [8], and separation processes [9].

The main synthesis routes for mesoporous solids like UVM-7 involve the formation of intermediates, and depending on these intermediates, different routes are followed. The most commonly employed method is the hydrothermal or sol-gel process, in which a surfactant, serving as a template for the gelification process, is dissolved (either in a basic or acidic medium). This results in the formation of a mesostructured material by self-assembly between surfactant micelles and silica oligomers under alkaline conditions, followed by template removal by calcination and consequent mesopore generation [10]. For this procedure, the atrane route is followed, which is a type of sol-gel process wherein the inorganic hydrolytic precursor is an atrane complex. Atranes can be easily prepared departing from alkoxides or salts by reaction with triethanolamine simply by heating. In the case of the alkoxides the heating

* Corresponding author.
E-mail address: J.Vicente.Ros@uv.es (J.V. Ros-Lis).

https://doi.org/10.1016/j.micromeso.2024.113314
Received 9 May 2024; Received in revised form 26 July 2024; Accepted 23 August 2024
Available online 26 August 2024

removes by evaporation the alcohol formed in the reaction [11]. Atranes, akin to alkoxides, are compounds employed as oxide precursors in the synthesis of mesoporous materials, but the distinction lies in their inertness towards hydrolysis. The versatility of this method makes it suitable for the preparation of mixed or doped mesoporous oxides [11]. This procedure encounters the challenge of distinct reactivities between heteroatoms, leading to phase mixtures. However, by using atranes as precursors the rates of hydrolysis and condensation of the different heteroelements can be balanced [12]. Another method/mechanism is the liquid-crystal templating mechanism (LCT), where the inorganic phase grows within the spaces between ordered organic micelles previously auto-organized [10]. Additionally, another approach is Evaporation-induced self-assembly (EISA), which involves the condensation and self-assembly of a metal-template composite via slow evaporation of non-aqueous organic solvents [13].

The integration of titanium into mesoporous silica matrices introduces additional functionalities and expands the potential applications of these materials. Titanium exhibits excellent catalytic activity, photocatalytic properties [1], and biocompatibility, making it a highly desirable component in various fields including environmental remediation [14], energy conversion [4], and biomedicine [15]. For some time now, studies have been carried out involving the incorporation of titanium on different supports, although mainly on mesoporous materials, since these provide wide pores that allow the easy entry and exit of reagents and products [16].

There are also numerous studies that coordinate other metals to the structure of these silicas to perform catalytic functions, such as gold [17, 18].

Microwaves have been widely applied in transmission of information and heating processes. They have been widely used in organic and inorganic synthesis [19–21]. Microwave assisted heating offers advantages such as rapid heating, improved reaction kinetics, providing a rapid and homogeneous energy transfer throughout the reaction mixture, resulting in shorter reaction times, improved product yields, and enhanced material properties [22]. Among the various microwave sources, the magnetron holds significant prominence due to its cost-effectiveness, simplicity, and high-power output. However, magnetron presents inherent limitations including challenges associated with power control, high voltage requirements, and limited operational lifespan [23]. By contrast, solid state microwave generators have emerged as an alternative to magnetrons with improved selection of parameters (potency, frequency and phase), and generate a precise and constant power. Despite these advantageous features, the relatively recent introduction of solid-state sources, their comparatively higher costs, and the absence of commercial equipment for chemistry synthesis using this technology have limited their widespread adoption and implementation [24].

Lately, the utilization of microwave solid-state generators has emerged as a promising alternative for the synthesis of various materials, including mesoporous silica materials such as MCM-41, SBA-15, SBA-16, etc. [21]. In 2023, Díaz de Greñu and coworkers reported for the first time the complete production of UVM-7 (synthesis, calcination and functionalization) using solid-state microwave generators [25], and subsequently the adaptation to obtain large quantities in scale-up and in flow systems was described by Benitez et al. They achieved a scaling factor of 100, with the obtention of 168 g per hour in scaled-up systems, and 59 g per hour with flow methods, adding the functionalization of 59 g per hour [26].

However, the use of solid-state microwave generators has not been validated for the preparation of mixed silica materials.

Thus, we hypothesize that solid-state based microwave assisted synthesis in combination with the atrane route can be an interesting approach towards a fast, scalable, and sustainable synthesis of mixed silica mesoporous materials, in particular titanium containing ones, such as Ti-UVM-7. The resulting materials would be homogeneous, with high Ti content, and with solar shielding properties.

2. Materials and methods

2.1. Chemicals

All the reagents were analytically pure and were used without further purification. Tetraethyl orthosilicate, 98 % (GC) (TEOS), triethanolamine ≥99.0 % (GC) ($TEAH_3$), hexadecyltrimethylammonium bromide ≥98.0 % (CTABr), and titanium(IV)butoxide, reagent grade, 97 % were purchased from Sigma Aldrich (Madrid, Spain). Ethanol was purchased from VWR. Deionized water was prepared in our lab. For the optical properties polymethylmethacrylate PMMA plates were used.

2.2. Microwave devices

Two different solid-state devices were employed, one designed for batch optimization and flow synthesis, and the other one for the batch scale-up, both supplied by Microbiotech. The low potency system, used for the optimization and flow synthesis, consists of a solid-state microwave source connected through coaxial cables to the irradiation cavity. The source can operate at a maximum power of 200W, with selectable potency in 5W increments. The frequency can be adjusted to fine-tune the system and optimize absorbed power within the 2420 MHz–2480 MHz range, in 1Hz increments. The scale-up batch device comprises four microwave sources interconnected through coaxial cables to the irradiation cavity. Each source can operate at a maximum power of 200W, with selectable potency in 1W increments, reaching a cumulative maximum power of 800W. The frequency of each source can be independently adjusted to fine-tune the system and optimize absorbed power within the 2420 MHz–2480 MHz range, in 1Hz increments, while maintaining phases within the 0-360° range.

2.3. Synthesis of the Ti-UVM-7 nanomaterials

The synthesis of Ti-UVM-7 was conducted via the atrane route [27] employing a one-pot procedure. For the batch optimization diverse Si/Ti molar ratios, potencies and reaction times were tested. They are summarized in Table 1. For example, for material having a nominal Si/Ti molar ratio of 25, a mixture containing 11 mL of TEOS, 23 mL of $TEAH_3$ and 0.7 mL of the Ti precursor was heated at 140 °C for 10 min to prepare the Si and Ti atrane complexes in $TEAH_3$ medium. The resulting solution was cooled to 90 °C and 4.7 g of CTABr was added, resulting in an anhydrous solution containing both the atrane precursor and the template agent. 4 mL of this atrane solution was introduced in a microwave glass vial together with 10 mL of deionized water. Subsequently, the vial was placed in a solid-state microwave oven cavity and irradiated for a specified duration at the defined power. The resulting white solid was washed with water and ethanol, followed by drying in an oven at 80 °C overnight to obtain the as-made material. Finally, the material is calcined at 550 °C for 6 h in a conventional furnace, obtaining Ti-UVM-7 mesoporous silica.

For the scaled-up synthesis, a strategy similar to the preparation of pure silica UVM-7 was followed [26]. To obtain the samples 18 and 19 (Si/Ti 50), the solution containing atranes was prepared with a mixture of 135 mL of TEOS, 263 mL of $TEAH_3$, 4.1 mL of $Ti(OBut)_4$, and 45 g of CTABr. The detailed procedure for the preparation of the atrane can be found in the previous paragraph. Subsequently, 1 L of miliQ H_2O was added to the atrane solution, placed into the microwave oven cavity, irradiated for 10 min at 800W, washed with water and ethanol, dried in an oven at 80 °C overnight and calcined at 550 °C for 6 h in a conventional furnace. This procedure was replicated both with and without stirring, to assess the influence of stirring on final product. For the samples 16 (Si/Ti = 10) and 17 (Si/Ti = 25), 125 mL of TEOS/19.3 mL of $Ti(OBut)_4$, and 132 mL of TEOS/8.2 mL of $Ti(OBut)_4$ were used, respectively.

In flow synthesis, the configuration of the system was similar has been reported elsewhere [19]. The atrane solution was prepared as in

Table 1
Summary of the main synthesis parameters.

Sample	Process type	TEOS (mL)	$Ti(OBut)_4$ (mL)	Si/Ti[a]	Power (W)	Time (min)
1	Batch	10.8	0.33	50	25	2:00
2	Batch			50	25	4:00
3	Batch			50	25	6:00
4	Batch			50	25	8:00
5	Batch	10.6	0.65	25	25	2:00
6	Batch			25	25	4:00
7	Batch			25	25	6:00
8	Batch			25	25	8:00
9	Batch	10.1	1.54	10	25	2:00
10	Batch			10	25	4:00
11	Batch			10	25	6:00
12	Batch			10	25	8:00
13	Batch	10.6	0.65	25	50	2:00
14	Batch			25	100	1:00
15	Batch			25	200	0:30
16	Batch, static	10.1	1.54	10	800	10:00
17	Batch, static	10.6	0.65	25	800	10:00
18	Batch, static	10.8	0.33	50	800	10:00
19	Batch, stirred	10.8	0.33	50	800	10:00
20	Flow	10.8	0.33	50	50	2:00
21	Flow	10.8	0.33	50	50	2:00
22	Flow	10.8	0.33	50	50	2:00
23	Flow	10.6	0.65	50	200	0:30
24	Flow	10.6	0.65	25	200	0:30

[a] Nominal molar ratio.

the batch synthesis, but the atrane (80 °C) and water (room temperature) were mixed using two peristatic pumps before its introduction in the microwave oven. This setup enabled controlled irradiation under varying time intervals and power settings. The peristaltic pumps were calibrated to ensure the precise blending of atrane and water, configured at 5 rpm for atrane and 12 rpm for water. The resulting precipitate was washed with water and ethanol, dried at 80 °C and calcined at 550 °C as before.

2.4. Characterization of the materials

Nitrogen adsorption–desorption isotherms were recorded using an automated Micromeritics ASAP2010 instrument. Prior to adsorption measurements, the samples underwent in situ outgassing in vacuum conditions (10^{-6} Torr) at 110 °C for 15 h to eliminate adsorbed gases. The specific surface area was determined utilizing the Brunauer–Emmett–Teller (BET model) based on adsorption data within the low-pressure range. Pore volume was calculated employing the Barrett–Joyner–Halenda model (BJH). The powder X-ray diffraction pattern (XRD) of the samples was acquired employing a D8 Advance A25 Bruker Corporation powder X-ray diffractometer. The sample underwent scanning across the requisite 2θ values range (1–80°). Transmission Electron Microscopy (TEM) was performed using a JEOL Jem 1010 instrument operating at 80 kV. HRTEM (high resolution transmission electron microscopy) images were acquired with a TECNAI microscope operated at 200 kV. Particle size analysis and Z potential for the samples were conducted using the Malvern Instruments Zetasizer Nano series particle size analyzer. The UV/visible spectrum was obtained through a PerkinElmer Lambda 35 spectrophotometer equipped with an integrating sphere. Raman spectra were obtained using a HORIBA Jobin Yvon iHR320 Spectrometer. X-ray photoelectron spectroscopy (XPS) measurements were collected with a SPECS spectrometer equipped with a Phoibos 150 MCD 9 analyzer and a nonmonochromatic Al Kα (1486.6 eV) X-ray source. Spectra were recorded at 25 °C using an analyzer pass energy of 30 eV, an X-ray power of 50 W, and under an operating pressure of 10^{-9} mbar.

2.5. Measurement of the optical properties

The Kubelka-Munk function and the Tauc plot method (see Equation (1)) were used to measure de band gap energy (Eg), where C is a constant, h is Planck's constant, v is the frequency of vibration and α is the absorption coefficient [28]. Representing the plot of $(hvf(R))^2$ vs photon energy (hv), where (f(R)) is the absorbance, the band gap energies can be calculated [28].

$$\propto(hv) = \frac{C(hv - E_g)^{\propto/2}}{hv} \quad (1)$$

Sun shielding properties were determined using the procedure of the European Cosmetic and Perfumery Association (COLIPA) [29]. Different amounts of Ti-UVM-7 were mixed with a moisturizing cream until a consistent paste, with sunscreen-like texture, were achieved. The resulting mixture was applied into the rough surface of the PMMA plate using a gloved finger, ensuring an even distribution, followed by compressed air for 1 min to eliminate any free particles. According to the Food and Drug Administration (FDA), PMMA plates are recommended because it is transparent to ultraviolet (UV) radiation, non-fluorescent, resistant to light degradation and inert to sunscreen ingredients [30]. The plate was then placed in a darkened environment for 15 min, allowing the sample to adapt and stabilize in a light-free setting. Finally, the transmittance was measured ten times in the range from 290 to 400 nm. Data were further analyzed to determine the UV protection calculating the Sunburn Protection Factor (SPF). SPF was calculated using equation (2), where E(λ) represents the Erythema Action Spectrum, I(λ) represents the sun's radiation power and T(λ) is the transmission for each wavelength.

$$SPF = \frac{\int_{290}^{400} E(\lambda)\cdot I(\lambda)\cdot d\lambda}{\int_{290}^{400} E(\lambda)\cdot I(\lambda)\cdot T(\lambda) d\lambda} \quad (2)$$

2.6. Data analysis and Life cycle assessment

The data analysis was performed using the IBM SPSS software version 28.0.1.1. Life Cycle Assessment (ISO 14040:2006) in a cradle to gate basis was applied to the scaled processes. The inventory was defined using the synthesis procedures and the energy consumption measured in the laboratory. The impact was calculated using the Ecoinvent 3 database and the ReCiPe 2016 Endpoint (H) V1.08/World (2010) H/A model available in the SimaPro software. If available data from Spain or Europe have been used. The method includes as impact categories global warming, stratospheric ozone depletion, ionizing radiation, ozone formation (human health), fine particulate matter formation, ozone formation (terrestrial ecosystems), terrestrial acidification, freshwater eutrophication, marine eutrophication, terrestrial ecotoxicity, freshwater ecotoxicity, marine ecotoxicity, human carcinogenic toxicity, human non-carcinogenic toxicity, land use, mineral resource scarcity, fossil resource scarcity and water consumption. CTABr is not available in the data base, thus, esterquat (a cationic surfactant) was used for the analysis. Titanium butoxide was modelled using the molar ratio in the reaction of titanium tetrachloride with butanol, and the energy calculated with the enthalpy of reaction. For the preparation of 1 Kg of titanium butoxide, 0.5 Kg of titanium tetrachloride, 0.87 Kg of 1-butanol, and 0.03 KWh of electricity were used, and 0.43 Kg of hydrochloric acid is generated as subproduct. The sunscreen was calculated following the composition detailed by the Joint Research Centre (JRC), the European Commission's science and knowledge service [31]. The inventory can be found in the supplementary material (Table S2).

3. Results and discussion

3.1. Synthesis procedure and optimization

Considering the goal of developing sustainable processes for preparing silica-based mixed porous materials, we opted for the combination of the atrane route with microwave-assisted synthesis. Titanium is particularly suitable as a proof of concept given its compatibility with silicium in the silica, as both can give rise to tetrahedral structures with oxygen, and the numerous applications of titanium dioxide.

The synthesis of silica modified with titanium faces the obstacle of different reactivities between the two heteroatoms, resulting in the formation of phase mixtures. To address this challenge, a potential solution is the use of atranes as hydrolytic precursors to control the rates of hydrolysis and condensation. Triethanolamine ($TEAH_3$) assumes an essential role in the synthesis of UVM-7. Its primary function is to form atrane complexes that modulate and balance the hydrolysis-condensation rate of Si and Ti. As a general rule, the synthesis of atrane complexes is carried out by transesterification reactions, starting from alkoxy derivatives in dry nonaqueous solvents. In our case, the Si and Ti atrane complexes were prepared together by heating the mixture of the corresponding commercial alkoxides in triethanolamine medium for a few minutes at 140 °C [11]. Additionally, when employed in excess, $TEAH_3$ can also act as a co-solvent in the synthesis process [32]. The porosity is promoted by CTABr as structure directing agent.

The synthesis procedure has been described in Fig. 1. For the batch synthesis, an atrane mixture with molar composition (2-x):x:7:0.52:180 of Si:Ti:$TEAH_3$:CTABr:H_2O is heated by the solid-state microwave generator. In a previous study conducted by our group, the synthesis of UVM-7 was performed using 200 W for 30 s, 100 W for 1 min, and 50 W for 2 min. In this work, with the incorporation of titanium, we have reproduced these procedures and additionally conducted synthesis at 25 W for 4 min. Characterization of these four samples revealed that the optimal results were achieved by heating for 4 min at 25 W [25]. Subsequently, we conducted further experiments using different durations at the same power level to observe any potential variations. Then, the reaction time was established between 0.5 and 8 min, a time markedly low considering that, up to our knowledge, the shortest reaction time reported for the synthesis of Ti-UVM-7 is 2 h [32]. The resulting suspension is filtered, washed, dried, and calcined to remove the surfactant from the pores to obtain the mixed oxide Ti-UVM-7 materials. Experimental conditions are summarized in Table 1. Reactions 1 to 15 were designed to evaluate the effect of the composition and operational parameters of the equipment in the properties of the materials. The rest correspond to the scaled-up reactions and will be discussed in the next section.

The main structural characteristics of the materials prepared have been collected in Table 2. The homogeneity of the materials was first studied by EDX and XRD in the range of 10 to 80° (2θ). EDX measures were used to analyze the sample composition and chemical homogeneity. As indicated in Table 2, the observed titanium content diverges significantly from the nominal values for all solid samples prepared in batch. A consistent tendency of titanium enrichment is evident. This trend can also be observed in the synthesis of Ti-UVM-7 using the conventional method [33], indicating it is not caused by the use of the microwave, but instead it is attributed to the higher solubility of silicon oxide (SiO_2) compared to titanium oxide (TiO_2). If we consider that the materials can be described as mixtures of SiO_2 and TiO_2 oxides, it is well known that the solubility of SiO_2 (ca. 0.12 g/mL) is much greater than that of TiO_2 (ca. 8.10–10 g/mL) [34,35]. After the hydrolysis of the respective atrane complexes, condensation reactions will take place and as the oligomers interact with the surfactant molecules, the Ti-UVM-7 particles will nucleate and grow. As the Ti content (x) of the pore walls increases (1-x SiO_2: x TiO_2 or Si_{1-x} Ti_xO_2) the titanium-rich domains will have a lower solubility than silica. Then, the Ti enrichment can be assigned to a partial silica dissolution. A similar trend was observed for other solids of the UVM-7 family containing Zr and Gd as heteroelements [36,37].

XRD at high angles shows a typical wide signal at ca. 20–30° (2θ) which corresponds to the amorphous silica phase [38]. It should be mentioned that no peaks corresponding to TiO_2 crystalline phases were found (Fig. 2b), suggesting the incorporation of Ti atoms into the silica structure probably occurs, in a majority way, through isomorphic substitution. This was confirmed with Raman (Fig. S1), where no peaks were found for TiO_2 anatase or rutile. Only those of SiO_2 appear [39].

Low angle XRD pattern provides information on the degree of ordering of the hexagonal porous array. Typically, the UVM-7 materials have a peak round 2° (2θ) corresponding to the plane 100 (hkl) and one weak shoulder associated with overlapped (110) and (200) planes, corresponding with an ordered hexagonal cell symmetry typical in mesoporous materials. We can observe that there are no appreciable changes in the (100) peak signal. The overall appearance of the diffractogram at low angles, including the shoulder associated with the superimposed (110) and (200) reflections, in general, does not change significantly with the titanium content at low to medium Ti contents (Fig. 2a). However, at large Ti content (Si/Ti = 10), although the (100) peak is observed the comparatively lower intensity suggests a loss of the large scale order of the porous system. This indicates that the variation in the Si/Ti ratio affects the particle morphology (see below) more than the XRD signal. A similar behavior has been observed for Ti-UVM-7 materials synthesized by the conventional method [33]. Probably, the ability of titanium to be largely incorporated into the silica network in environments with tetrahedral geometry implies less distortion of the mesostructure than that observed when heteroelements other than Ti

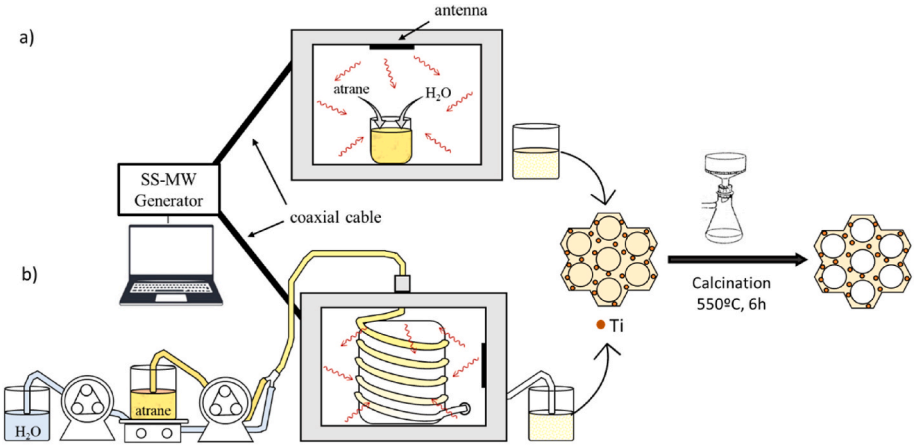

Fig. 1. Synthesis procedure scheme in (a) batch, and (b) flow.

Table 2
Selected synthetic and physical data for Ti-UVM-7 bimodal porous materials prepared in the batch optimization.

	Si/Ti[a]	Si/Ti[b]	S_{BET} (m^2 g^{-1})	Mesoporous diameter[c] (nm)	Textural pore diameter[c] (nm)	Mesoporous volumen[c] (cm^3 g^{-1})	Textural pore volume[c] (cm^3 g^{-1})	ζ[d] (mV)	2θ (°)	d_{100}[e] (nm)	a_0[f] (nm)	Wall thickness[g] (nm)
1	50	13.8 ± 0.7[a]	819 ± 3	2.4	20.8	0.37	0.34	−29.1 ± 0.6[a]	2.27	3.9	4.5	2.1
2	50	21.2 ± 0.5[b]	764 ± 2	2.5	20.8	0.37	0.31	−35.7 ± 0.9[b]	2.35	3.8	4.3	1.6
3	50	20.7 ± 0.8[bc]	879 ± 4	2.6	18.5	0.51	0.52	−27.3 ± 0.3[c]	2.31	3.8	4.4	1.9
4	50	24.7 ± 1.7[c]	889 ± 2	2.6	22.2	0.56	0.75	−29.6 ± 1.9[a]	2.27	3.9	4.5	1.7
5	25	3.6 ± 0.2[a]	985 ± 4	2.8	26.2	0.75	0.84	−28.7 ± 0.7[a]	2.00	4.4	5.1	2.3
6	25	4.3 ± 0.2[a]	786 ± 2	2.5	41.1	0.45	0.58	−30.0 ± 0.6[a]	2.02	4.4	5.1	2.5
7	25	11.4 ± 0.6[b]	864 ± 3	2.5	21.3	0.52	0.49	−35.1 ± 1.3[bc]	2.31	3.8	4.4	1.9
8	25	13.5 ± 0.6[c]	902 ± 2	2.9	26.1	0.71	0.65	−33.6 ± 1.7[ab]	2.27	3.9	4.5	1.6
9	10	2.0 ± 0.0[a]	454 ± 3	2.3	24.9	0.11	0.12	−33.5 ± 0.9[ab]	–	–	–	–
10	10	3.5 ± 0.3[b]	542 ± 2	2.4	26.0	0.19	0.29	−31.1 ± 0.9[bc]	–	–	–	–
11	10	3.8 ± 0.2[b]	585 ± 2	2.4	25.7	0.23	0.23	−25.3 ± 0.5[d]	2.29	3.9	4.5	2.0
12	10	3.9 ± 0.2[c]	738 ± 2	2.5	23.2	0.35	0.45	−26.6 ± 0.6[cd]	2.37	3.7	4.3	1.8
13	25	7.3 ± 0.3[d]	879 ± 3	2.5	38.2	0.49	0.35	−28.8 ± 1.3[a]	2.11	4.2	4.8	2.4
14	25	8.4 ± 0.4[e]	903 ± 4	2.5	39.2	0.52	0.38	−32.2 ± 0.4[ab]	2.12	4.2	4.8	2.4
15	25	8.7 ± 0.3[e]	788 ± 2	2.5	32.9	0.39	0.30	−39.2 ± 0.8[c]	2.15	4.1	4.7	2.3

where n is the diffraction order, λ is the wavelength of the incident X-rays and θ is the diffraction angle.

[a] Theorical mixture.

[b] Real mixture determined by EDX, letters indicate groups assigned by Tukey post hoc analysis within the materials with the same Si/Ti theoretical mixture (p = 0,05).

[c] BJH pore sizes estimated from the isotherms adsorption branch.

[d] Zeta potential, letters indicate groups assigned by Tukey post hoc analysis within the materials with the same Si/Ti theoretical mixture (p = 0,05).

[e] Distance between planes of the hkl 100, calculated by $d_{100} = n \cdot \lambda \cdot (2\text{sen}\theta)^{-1}$.

[f] Cell parameter calculated by $a_0 = d_{100} \cdot (\sqrt{3})^{-1}$.

[g] Wall thickness was calculated by $dw = a_0\text{-}dp$, where dp is the mesopore diameter.

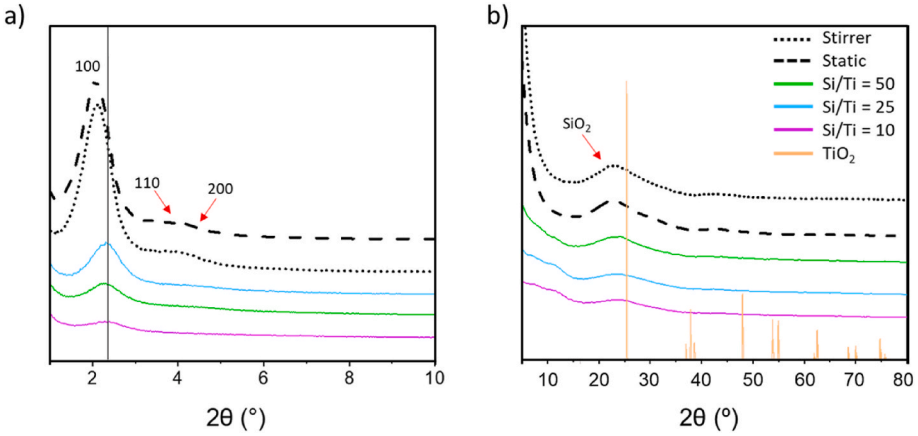

Fig. 2. XRD at a) low angles, and b) high angles of representative samples.

are inserted. Undoubtedly, the fact that it has a formal charge identical to that of silicon (IV), together with its stabilization in tetrahedral environments, favors its isomorphic substitution (over a wide range of concentrations) and therefore less modification of the initial mesostructure of silica. At a glance, from the information in the table, it can be deduced that an ordered pore structure can be obtained for all the concentrations tested. However, as the concentration of titanium increases, it is necessary to use longer irradiation times. In any case, 6 min is sufficient reaction time for material with a lower Si/Ti ratio. From the N_2 adsorption/desorption isotherm, we obtain type IV adsorption-desorption plots, typical of mesoporous solids (Fig. 3a). They present two adsorption steps, the first at medium relative pressures

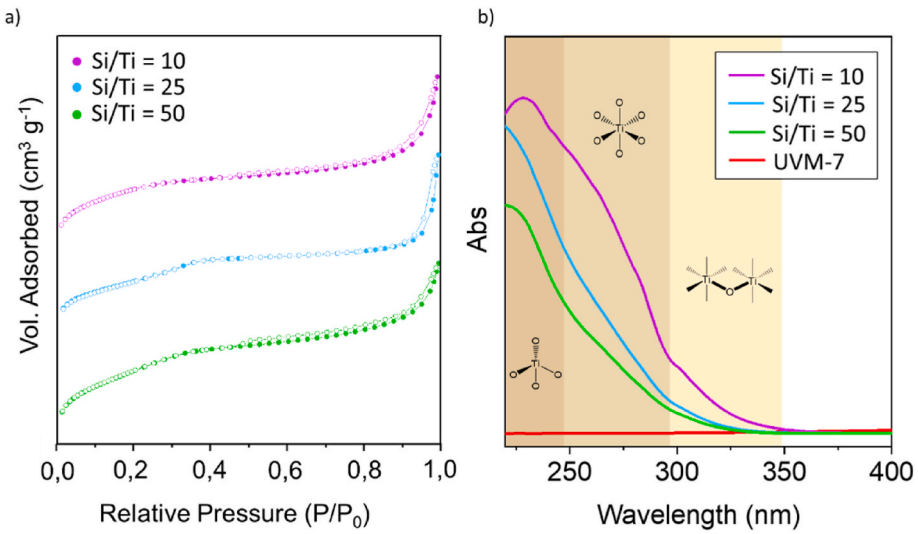

Fig. 3. a) N_2 adsorption-desorption isotherms of samples 3, 7 and 11, and b) UV absorption, with diverse Si/Ti ratios.

between $0,2 \leq P/P_0 \leq 0,4$ which can be associated with a mesopore system, and the second one, at high relative pressures between $0,9 \leq P/P_0 \leq 1,0$ which is due to a large-meso or macropore system. All materials, even those without peaks at low angles in XRD, show isotherms with the bimodal pore structure typical of UVM-7, with a mesopore of 2–3 nm, and a textural large pore in the 20–40 nm range. Although a similar mesopore size is observed for all materials, in general, Ti-UVM-7 prepared with a shorter irradiation time presents differentiated structures with compared to the rest with a larger pore wall size. The area decreases due to the incorporation of titanium to values around 800 $m^2 g^{-1}$, which is consistent with previous results in which the UVM-7 area decreases when other elements are incorporated [40].

In general, all materials exhibit high values of Z potential, around −30 mV. As the Z-potential is farther away from zero, the suspension is more stable, less likely to aggregate. Thus, these potentials are particularly suitable for obtaining more suspendable materials and are slightly higher than those observed for pure silica UVM-7 [40]. This increase in potential can be understood if we take into account that Ti is more acidic than Si [41], therefore in the presence of Ti, it is easier to deprotonate the OH groups, generating a greater negative charge on the surface of the material.

ANOVA with Tukey post hoc analysis applied to those materials with the same nominal Si/Ti ratio indicate that the irradiation time is able to generate materials with diverse Si/Ti ratios and Z potential, and these differences are statistically significant (Table 2, $p = 0.05$). To better understand the influence of the different variables on the textural characteristics and composition of the materials obtained, a linear adjustment was carried out, considering the Si/Ti relationship, power and time as independent variables, and the area and other characteristics of Table 2 as dependent variables. It is evident that irradiation time primarily influences the amount of titanium incorporated into the matrix. There is a clear trend indicating that increased irradiation time leads to higher titanium enrichment in the samples. With shorter irradiation times in the microwave cavity, the material contains a higher amount of TiO_2. This occurs because SiO_2 is more soluble than TiO_2, resulting in greater dissolution of SiO_2 and less incorporation into the solid compared to TiO_2. A summary of the degree of significance for the different variables can be found in Table S1 of the Supplementary material. For a degree of significance of $p < 0.1$, in the case of the measured Si/Ti ratio, the main parameter is the nominal Si/Ti ratio, although the reaction time is also decisive. When the reaction time increases, there is a reduction in the titanium content. In the case of textural parameters determined from N_2 adsorption/desorption, the surface area depends fundamentally on the Si/Ti ratio, decreasing with increasing Ti concentration. Mesopore diameter, textural pore, and textural pore volume depend on the Si/Ti ratio and reaction time, with positive correlations. On the contrary, the textural pore diameter does not depend on the variables analyzed, corresponding to uncontrolled or random factors. Z-potential and cell size are other parameters that do not depend on the variables tested. Finally, the size of the wall, since it is related to the pore size, also depends on the Si/Ti ratio and the irradiation time.

As a complement to the above techniques, electron microscopy provides an overview of the morphology of the material. TEM images reveal the typical UVM-7 structure of this class of materials for the samples with Si/Ti nominal molar ratios of 50 or 25, consisting in small mesoporous particles that assemble, resulting in the formation of large textural pores among them (Fig. 4b). The study with different irradiation times and potencies (samples 6 and 13 to 15), showed similar structures, confirming that the reaction time can be significatively reduced to less than 1 min. However, when the Si/Ti ratio is 10 (samples 9 to 12), a morphological transformation occurs in the particles. Pores are less readily discernible compared with the rest of materials, particularly in sample 9. In addition, a segregation of phases is observed, finding dense phases with a crystalline appearance surrounded by a material with the characteristic appearance of porous silica (Fig. 4a), which have a disordered structure according to the XRD data recorded at the low-angle range. It should be borne in mind that the titanium content is very high (Si/Ti real molar ratio less than 4), which would modify the structure of the material excessively, even at long reaction times, resulting in a heterogeneous material. In the HRTEM images (Fig. 5), samples with a Si/Ti nominal molar ratio of 10 exhibit an appreciable particle size heterogeneity together with small spots attributed to Ti-rich domains of sizes around 9 ± 3 nm. In contrast, samples with a lower Si/Ti nominal molar ratio show a particle size homogeneity typical of pure silica UVM-7 materials and even smaller (5 ± 3 nm) and more homogeneously distributed Ti-rich nanodomains within the porous silica matrix. This observation corroborates the XRD findings, indicating that variations in the Si/Ti ratio significantly affect particle morphology. No order is observed in the titanium-rich domains. Their small size, even if they were TiO_2 nanoparticles, excludes their detection by X-ray diffraction. This is consistent with the absence of peaks in the high-angle XRD patterns.

Finally, the effect of titanium incorporation on the local structure can be confirmed by UV–Vis and XPS. In all cases, the UV–Vis spectra of the final mesoporous materials (Fig. 3b) show an intense adsorption in the 214–225 nm range, which is typically assigned to a ligand to metal charge transfer involving isolated and tetrahedrally coordinated Ti atoms [42]. Notwithstanding, the significant adsorption tails in the

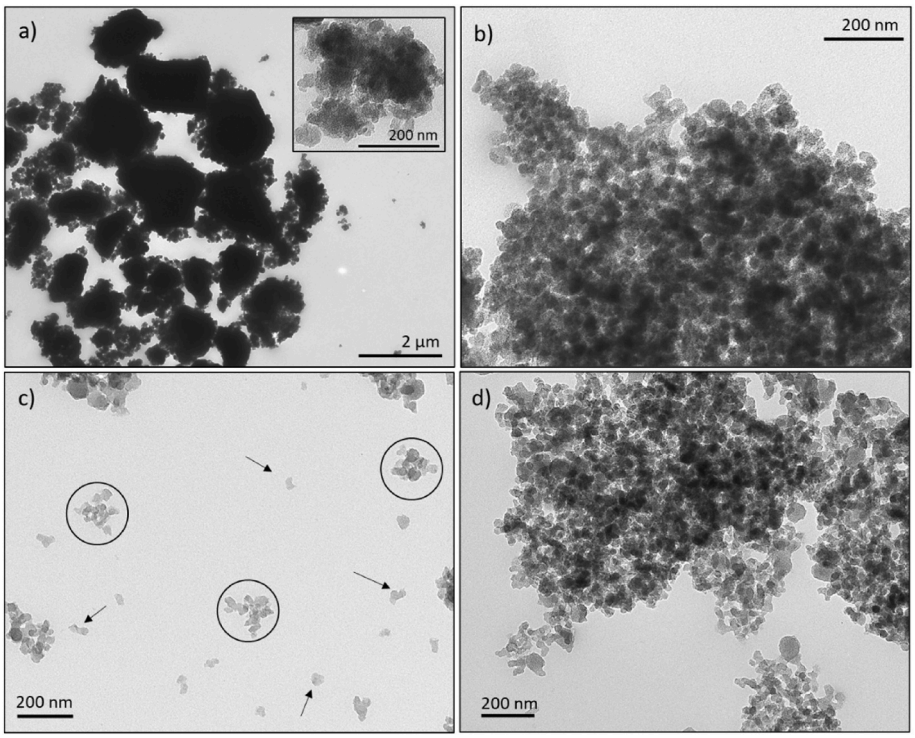

Fig. 4. TEM images for a) sample with a Si/Ti molar ratio of 10 (sample 11), b) sample with a Si/Ti molar ratio of 25 (sample 7), c) scale-up sample with stirring, and d) scale-up sample without stirring. The presence of aggregates of smaller nanoparticles in the case of the scale-up sample with stirring is indicated with circles and arrows.

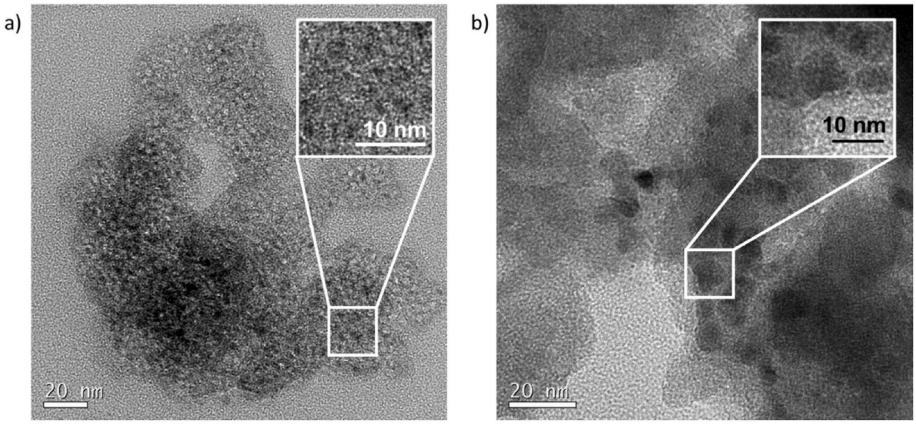

Fig. 5. HRTEM images of a) sample 7, and b) sample 11, showing the darker domains associated with regions richer in Ti (marked with arrows). High magnification images focusing on these domains are presented in the insets.

250–350 nm range (whose intensity increases with the Ti content) further indicate the presence of octahedral environments for Ti [43]. At this point, it has to be noted that none of the samples causes appreciable absorption at $\lambda > 350$ nm, which, in principle (in good agreement with the XRD results) would be compatible with the single-phase nature of all these solids (i. e. this technique also fails to suggest the presence of extra-framework TiO_2 crystalline domains) [44]. In the samples with lower Ti content, the typical Ti signal in tetrahedral environments is dominant. As the heteroelement concentration increases, the intensity of this signal increases and a certain adsorption appears at lower energy associated with Ti atoms in octahedral environments.

The Ti2p, O1s and Si2p core level XPS spectra of three representative samples with variable amounts of titanium (samples 3, 7 and 11; $3.8 \leq$ Si/Ti real molar ratio ≤ 20.7) have been recorded (Fig. 6). The binding energies (BE) of the Ti2p3/2 and Ti2p1/2 bands were observed to be within the range of 460.3–460.9 eV and 465.8–466.6 eV, respectively. These values are clearly somewhat higher than those typically observed for TiO_2 particles (459.3 and 465.2 eV) [45]. The Ti2p BE values observed in our materials fall within the range described for amorphous mixed oxides of Si and Ti [46] and also for solids of the Ti-MCM-41 type [47], which is in accordance with expectations. In the case of the sample with the highest titanium content, in addition to the two aforementioned signals, an additional Gaussian centered at 531.5 eV is required in order to achieve a satisfactory fit. As evidenced in the literature [46,48], an increase in titanium content in related systems is associated with a shift in binding energy (BE) values towards lower energies. It was observed that the contribution of the Gaussian to higher BE exhibited a decreasing trend with increasing Ti content. The respective percentages are 70, 63 and 35 % for samples 3, 7 and 11. Concurrently, the contribution of the Gaussian centered at 533.5 eV increases in proportion to the Ti content.

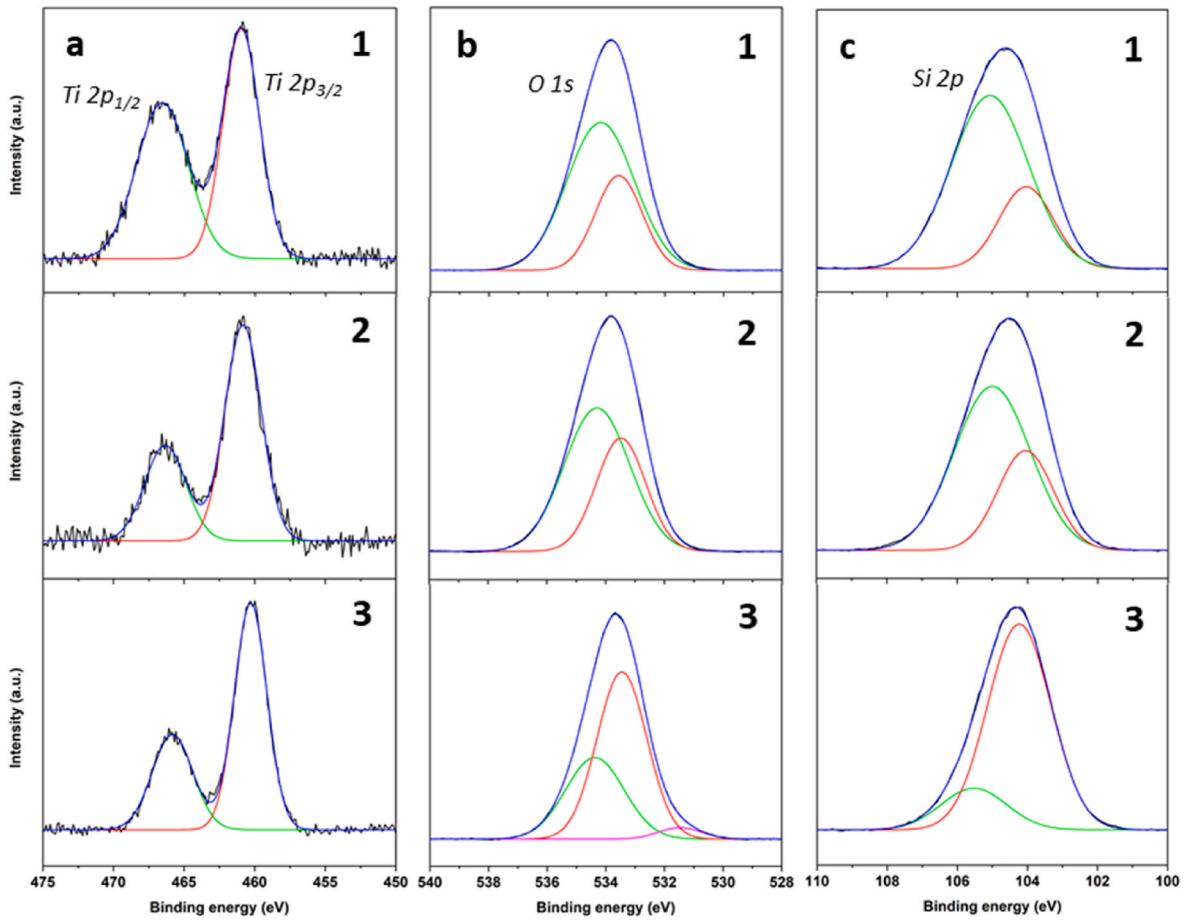

Fig. 6. a)Ti 2p, b) O 1s and c) Si 2p XPS spectra of sample 3 (1), 7 (2) and 11 (3).

The respective percentages are 30, 37 and 61 % for samples 3, 7 and 11, respectively. Moreover, in the case of the material with a higher Ti content, the deconvolution of the XPS O1s spectrum indicates the presence of an additional signal, contributing 4 % to the overall result. As the binding energy (BE) decreases, the local O environments evolve from Si-O-Si to Ti-O-Ti, passing through mixed environments of the Si-O-Ti type. In no case do the BE values approach those typical for TiO_2 (ca. 530 eV). The deconvolution of the XPS Si2p spectra has been performed on a consistent basis with two Gaussian functions centered at ca. 104 and 105 eV. The contribution of both evolves inversely, from 25 % (sample 3) to 83 % (sample 11) for the function centered at 104 eV (Si environments with nearby Ti atoms) and from 75 % (sample 3) to 17 % (sample 11) for the one centered at 105 eV (Si environments preferably surrounded by Si). The data obtained from the UV–Vis and XPS analyses are in accordance with the presence of a mixed oxide of silicon and titanium, exhibiting a highly uniform distribution of both elements and the absence of TiO_2 domains. Ti is predominantly located in environments with tetrahedral geometry (isomorphic substitution of Si), and as its concentration rises, it can be stabilized in octahedral environments, resulting in the formation of Ti-rich nanodomains.

From the above data, it can be concluded that microwaves of solid-state generators are a suitable technique for the preparation, not only of pure silica UVM-7 mesoporous materials, but also mixed silicas including other elements. In this case, Ti-UVM-7 type materials with Si/Ti ratios close to 4 can be obtained without phase segregation and preserving the typical topology of these materials. Also, it is noteworthy the fact that these materials can be prepared with only 30 s of irradiation.

3.2. Batch scale-up and flow and synthesis

To evaluate the possibility of preparing large quantities of Ti-UVM-7 we followed two approaches, batch scaling and flow synthesis. The first is *a priori* more feasible, although the limited penetration capacity of microwaves can generate difficulties when the size of the reactor increases, and there is a risk of having cold and hot spots. To avoid these drawbacks, flow synthesis enables the maintenance of a small conduction size, achieving homogeneous irradiation, and eliminating the presence of hot and cold spots through continuous movement. Also, the flow synthesis process can be easily automated.

Considering the objective of scaling the synthesis 100 times and given that the power of the equipment is limited to 800W, it was not possible to increase it proportionally with the increase in scale and it was decided to increase the reaction time to 10 min. Batch-scaled synthesis has been executed without stirring, in agreement with the optimization process in the previous section, and with the aim of a simpler implementation. A summary of the synthesis conditions can be found in Table 3 (samples 16 to 19). In flow synthesis, reactants are continuously introduced into the system and products are continuously removed (Table 3, samples 20 to 24). The main difference between batch and flow synthesis lies in the fact that, in the former, all reactants are combined in a single vessel and introduced into the reactor. Conversely, flow synthesis involves two solutions: one containing the atrane complexes and the template, and the other one the water. By employing two peristaltic pumps, the solutions are brought into contact just prior to entering the microwave system, with distinct flow rates selected to ensure the desired residence time within the reactor. Table 3 collects the main morphological parameters and composition of the scaled-up materials.

A first differentiating aspect in materials prepared by scaled

Table 3
Selected synthetic and physical data for Ti-UVM-7 bimodal porous materials prepared in the scale-up.

Sample	Si/Ti[a]	Si/Ti[b]	S_{BET} (m^2 g^{-1})	Mesoporous diameter[c] (nm)	Textural pore diameter[c] (nm)	Mesoporous volumen[c] (cm^3 g^{-1})	Textural pore volume[c] (cm^3 g^{-1})	ζ[d] (mV)	2θ (°)	d_{100}[e] (nm)	a_0[f] (nm)	Wall thickness[g] (nm)
16	10	8.2 ± 1.4	964 ± 4	2.7	36.5	0.74	0.94	−27.5 ± 0.6	2.15	4.1	4.7	2.0
17	25	22 ± 3	885 ± 3	2.7	50.2	0.70	1.75	−27.4 ± 0.6	2.11	4.2	4.8	2.1
18	50	49 ± 7	907 ± 2	2.8	35.0	0.77	0.77	−28.1 ± 0.4	2.07	4.3	4.9	2.1
19	50	50 ± 9	1041 ± 2	2.9	45.6	0.91	1.16	−28.6 ± 0.2	2.13	4.2	4.8	1.9
20	50	23.9 ± 0.7	1043 ± 6	2.7	20.2	0.79	0.67	−31.1 ± 0.5	2.47	3.6	4.1	1.5
21	50	25.1 ± 0.8	1070 ± 5	2.7	23.2	0.83	0.85	−31.5 ± 0.8	2.37	3.7	4.3	1.6
22	50	24.6 ± 0.6	1039 ± 7	2.7	25.0	0.77	0.88	−24.8 ± 0.4	2.37	3.7	4.3	1.6
23	50	46 ± 7	1039 ± 2	2.7	29.9	0.87	1.18	−29.4 ± 1.2	2.39	3.7	4.3	1.5
24	25	29 ± 2	1047 ± 3	2.7	42.0	0.85	1.60	−31.1 ± 0.9	2.41	3.7	4.2	1.5

where n is the diffraction order, λ is the wavelength of the incident X-rays and θ is the diffraction angle.
[a] Theorical mixture.
[b] Real mixture determined by EDX.
[c] BJH pore sizes estimated from the isotherms adsorption branch.
[d] Zeta potential.
[e] Distance between planes of the hkl 100, calculated by $d_{100} = n{\cdot}\lambda{\cdot}(2\text{sen}\theta)^{-1}$.
[f] Cell parameter calculated by $a_0 = d_{100}{\cdot}(\sqrt{3})^{-1}$.
[g] Wall thickness was calculated by dw = a_0-dp, where dp is the mesopore diameter.

synthesis is that there is a slight shift of the 100 (hkl) XRD peak toward lower angles, indicating an increase in cell size. However, unlike samples 13 to 15, in the scaled-up synthesis this variation can be assigned to an increase in pore size, with a lower contribution from wall size. Again, none of the materials showed the presence of the characteristic XRD peaks of TiO_2 in the high-angle domain (Fig. 2b), reinforcing the idea that Ti is effectively included in the silica network, which was also confirmed by Raman spectroscopy. The area and pore size are similar to the non-scaled-up synthesis. However, the pore volume increases, suggesting structural modifications that will be further analyzed by TEM. EDX data reveal that in the scaled synthesis nominal and measured Si/Ti ratios are similar.

In general, all materials exhibit high values of Z potential as before. We can observe that all values approach approximately −30, but in some cases, a slightly decrease can be observed. According to a study conducted by Esin Yakin, F. in 2020, the zeta potential depends on the particle size and porosity, showing a decrease of up to 10 % in the zeta potential when decreasing the particle diameter [48]. The TEM images of samples 16 to 19 show a UVM-7 structure for all materials, even those with a higher titanium content (Si/Ti = 10). It should be noted that sample 16 has a ratio of 8.2, similar to the non-scaled Si/Ti 25 that maintain the UVM-7 structure and incorporate Ti in a homogeneous way.

Regarding the effect of stirring (samples 18 and 19), only minor variations have been found in the textural properties, lower than the natural variability of this type of synthesis [25]. However, a slightly lower tendency to aggregation is observed in the reaction with agitation, obtaining a greater number of small particles (Fig. 4c,d).

Thus, the synthesis can be scaled-up in batch conditions maintaining the main features of the materials, in only 10 min. In each batch, approximately 33 g of calcined Ti-UVM-7 are obtained, a large amount considering that the process is fast, and it is prepared in a bench equipment.

In an alternative approach, the flow synthesis departing of atrane and water mixtures was also studied. Three experiments were conducted. First, the material was collected at different intervals in order to evaluate the homogeneity of the materials obtained in different synthesis intervals (samples 20 to 22). The second studied the effect of reducing the reaction time with equal energy (sample 23). Finally, we evaluated the possibility of using the same procedure to obtain a material with an intermediate titanium concentration (Si/Ti = 25, sample 24). From the data collected in Tables 2 and 3, compared to samples obtained in unscaled batch, flow samples show similar cell and pore sizes. However, the area is larger, exceeding 1000 m^2 g^{-1}. These values are common for UVM-7 materials [33], although higher than those obtained in the batch samples. If we check the parameters measured for samples 20 to 22 collected from the reactor at different times, we can see that they all present very homogeneous values, which supports the possibility of using microwave-assisted flow reactors for the preparation of mesoporous silicas containing titanium. In the above samples, 2 min were chosen because of its similarity to the reaction conditions tested in section 2.1, however, it appears that the reduction in reaction time has a dramatic effect on the incorporation of titanium into the silica structure. When we increase the flow 4-fold and thus the dwell time in the microwave oven decreases from 2 min to 30 s, the Si/Ti ratio values measured by EDX approximate the nominal values added in the reaction mixture (samples 23 and 24). This phenomenon will require further research in the future, but it is similar to what we have found in the batch scaling process. Finally, the data from samples 23 and 24 suggest that the synthesis procedure can be applied for the preparation of samples with variable titanium contents, at least up to a Si/Ti ratio of 25. TEM photos show a typical UVM-7 structure. 0.2 g of Ti-UVM-7 min^{-1} is obtained, which is equivalent to 12 g h^{-1}. As with batch scaling, the synthesis procedure described for the preparation of mixed porous silicas can also be adapted to flow synthesis.

3.3. Optical properties of Ti-UVM-7

TiO_2 is an excellent photocatalyst, typically it shows a band at 350 nm [49]. By contrast, pure silica UVM-7 is transparent in the UV–vis zone. In general, materials of Ti-UVM-7 absorb below 300–350 nm, indicating relatively large bandgaps, in agreement with the presence of

Titanium but the absence of TiO_2 nanodomains (Fig. 3b). These values are similar to titanium containing UVM-7 materials prepared by conventional procedures [33]. All the Ti-UVM-7 materials have bandgaps between 4 or 5 eV, in comparison with TiO_2 that has a value of 3.5 eV. When the Ti content increases it is observed a lower gap, with values of 4.9, 4.6 and 4.1 eV for the nominal molar ratios Si/Ti = 50, 25 and 10, respectively. However, the sample 9, with higher phase segregation, has a bandgap value of 3.80 eV, closer to the value for the TiO_2. Samples 20 to 24, synthesized under flow conditions, have a bandgap of 4.2 eV. This value is relatively low in comparison with the Ti-UVM-7 materials with similar Si/Ti ratio. As expected, Ti-UVM-7 samples with higher Ti content show stronger UV absorption, but also the textural properties can be relevant.

Considering these properties, we evaluated the properties of Sample 8 as suitable sunscreen material. Also, a commercial TiO_2 and pure silica UVM-7 were measured for comparison. The values of SPF have been collected in Table 4. We have calculated SPF values of up to 2.4 for a mixture with a 10 % of nanomaterial. This value can seem low if we consider that 5–10 % TiO_2 nanoparticles can offer SPF values between 6 and 9 [50]. However, if we consider only the Ti content, Ti-UVM-7 materials would be more effective than pure TiO_2 as sun shielding materials. The effect of Ti would be complemented with the effect of the UVM-7 structure, since SiO_2 is transparent to the UV radiation [51]. Additionally, some studies have reported that the incorporation of UV filters into mesoporous silica materials enhances the protective capacity of these compounds. A test was also conducted with 5 % UVM-7 without titanium, resulting in an SPF of 1. This result is consistent with that obtained by C.C. Li using 2 % mesoporous silica [52], and with Y.W. Cheng, who achieved an SPF of 1.1 using 4 % of the material [53], indicating the absence of significant photoprotection.

Although, 5 % Ti-UVM-7 has a SPF value higher than 5 % UVM-7 the differences are not statistically significant ($p = 0.05$). Barbosa, J.S [54]. conducted experiments to measure SPF of commercially available TiO_2 and SiO_2-coated TiO_2, both with a concentration of 4 wt%. The results indicated SPF values of 1.66 and 1.9, respectively, which closely aligns with the outcomes of our own investigation. With 1.8 % TiO_2, an SPF of 4 is achieved, which is double that obtained with 2 % TiO_2 without the mesoporous silica matrix. Using 10 % TiO_2 embedded in an SBA-15 matrix, Da Silva Marcelino achieved an SPF of 15 ± 1 [55]. This value is higher than in our case, but it must be considered that a larger amount of titania is present. If we consider the SPF/%TiO_2 ratio, the data we have obtained, aligns closely with the results for the SBA-15 material.

By means of the guidelines provided by the FDA, there exist restrictions on the percentage of anatase crystalline polymorph present in titanium dioxide to minimize its photocatalytic activity. The potential occurrence of photocatalytic activity poses a risk of degrading other active ingredients present in sunscreen products containing nanoscale titanium dioxide upon exposure to light. Extensive studies on TiO_2 have been conducted, focusing on product evaluations with TiO_2 concentrations up to 10 %. These concentrations have been generally acknowledged as safe and effective for use in sunscreens, with permissible concentrations reaching up to 25 % [54]. However, by using Ti coated in the UVM-7, this issue can be avoided.

The integration of titanium within the mesoporous silica matrix could enhance UV blocking capabilities, but also offers additional benefits such as enhanced stability, increased photoactivity, and improved photostability. Furthermore, the unique structural properties of mesoporous materials, characterized by a well-defined pore structure and high surface area, allow for the efficient incorporation of UV filters, promoting uniform dispersion and optimal UV absorption [56].

Table 4
Results of the SPF measurements for different amounts of Ti-UVM-7.

Material	% (w/w)	SPF ± SD	% TiO_2[a]
Ti-UVM-7	1	1.2 ± 0.3	0.08
Ti-UVM-7	5	1.6 ± 0.4	0.35
Ti-UVM-7	10	2.4 ± 0.9	0.68
Ti-UVM-7	30	4.0 ± 0.6	1.81
TiO_2	2	2.1 ± 0.9	2.00
UVM-7	5	1.08 ± 0.16	0.00

[a] TiO_2 equivalent calculated from the measured Si/Ti and the percentage of material used.

3.4. Life cycle assessment

The main advantage of microwaves is their efficiency in reducing reaction times. A reduced reaction time, combined with the use of low powers, enables a synthesis process with a lower energy consumption. The LCA was applied in a cradle to gate basis. The goals are the quantification of the global impact and main impact factors associated with the preparation of Ti-UVM-7 materials, evaluate the effect of the scale-up, and identify the main processes/reagents to suggest improvements. The functional unit was defined as the preparation of 1 kg of material.

The single score offers a general mark of the impacts. The non scaled-up synthesis offers a value of 245 points. This value is high, but it should be noted that in the laboratory process the small batch size implies a use of materials and processes that are not representative of the value on a large scale. Thus, in batch-scaled synthesis this value is reduced to 10.7 points, a value similar to that obtained in flow synthesis. The single score decreases to 2.7 points for 1 kg of sunscreen cream with a 25 % of loading of the Ti-UVM-7 material. As can be seen in Fig. 7a, for Ti-UVM-7 reactants, solvents, and energy are of similar importance. Therefore, the process could be improved by using energy with a lower environmental impact, removing or at least reducing the use of ethanol, and replacing reagents with lower-impact ones. This last point can be especially tricky since the main reagent is triethanolamine, a key reagent in the atrane route, but a reduction in the amount of triethanolamine could be studied. Also, the possibility of using novel sources of silicon, or more sustainable surfactants could be interesting topics for future works. Titanium butoxide offers an impact higher than TEOS, thus the use of inorganic titanium salts instead of titanium butoxide could be also advisable. Regarding the main impact categories, the main ones are Human carcinogenic toxicity, Freshwater ecotoxicity, Marine ecotoxicity, Freshwater eutrophication, and Ionizing radiation (see Fig. 7b), all of them related to the preparation of solvents and chemical reagents. By contrast, other relevant factors in impact studies such as global warming potential, or water consumption offer only a minor contribution, highlighting the relevance to perform full LCA studies to evaluate the processes, not only evaluations of single impact categories.

4. Conclusions

We have effectively demonstrated that the combination of the atrane route with the microwave assisted synthesis using solid-state generators can be an interesting approach to obtain, not only porous silica, but also mixed compound with other elements. In this study, we present for the first time the synthesis of Ti-UVM-7 successfully using a solid-state microwave generator in less than 10 min with a Ti content of up to 3.8 (Si/Ti real molar ratio). In some cases, the materials can be obtained in only 30 s. The microwave-assisted synthesis enabled efficient heating and precise control over reaction parameters, leading to the formation of Ti-UVM-7 with well-defined mesoporous structures and uniform titanium distribution. Regarding the operative parameters, the reaction time and Si/Ti ratio are significant. The reaction can be effectively scaled-up in batch and adapted to flow synthesis maintaining the typical UVM-7 topology. This allows the preparation of hundreds of grams with a significant reduction in the impact to only 10 points in the single score of LCA per kg of Ti-UVM-7, that could be reduced in an industrial process and/or modification of the reagents. The inclusion of Ti modifies the optical properties, reducing the band gap of the material favoring the use of this type of materials as sunscreens.

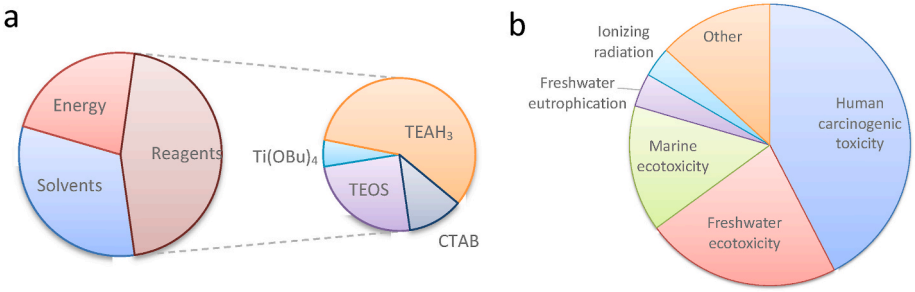

Fig. 7. Life Cycle Assessment. a) Contribution of the processes to the single score (Pt) of the scaled-up batch synthesis calculated following the ReCiPe 2016 Endpoint (H) V1.08/World H/A method. b) Main normalized impact category indicators of the scaled-up batch synthesis calculated following the ReCiPe 2016 Midpoint (H) V1.08/World (2010) H method.

CRediT authorship contribution statement

Cristina Rodríguez-Carrillo: Writing – review & editing, Writing – original draft, Methodology, Investigation, Conceptualization. **Miriam Benítez:** Writing – review & editing, Writing – original draft, Methodology, Investigation, Conceptualization. **Marta González-Fernández:** Investigation. **Ruth de los Reyes:** Investigation. **Sonia Murcia:** Visualization, Investigation. **Jamal El Haskouri:** Writing – review & editing, Writing – original draft, Investigation, Conceptualization. **Pedro Amorós:** Writing – review & editing, Writing – original draft, Supervision, Methodology, Investigation, Funding acquisition, Conceptualization. **Jose V. Ros-Lis:** Writing – review & editing, Writing – original draft, Supervision, Investigation, Funding acquisition, Conceptualization.

Declaration of competing interest

The authors declare the following financial interests/personal relationships which may be considered as potential competing interests:

Jose V. Ros-Lis reports financial support was provided by Spain Ministry of Science and Innovation. Jose V. Ros-Lis reports financial support was provided by Government of Valencia. If there are other authors, they declare that they have no known competing financial interests or personal relationships that could have appeared to influence the work reported in this paper.

Data availability

No data was used for the research described in the article.

Acknowledgments

This research was funded by the Spanish Ministerio de Ciencia, Innovación y Universidades, grant number PID2021-126304OB-C43 funded by MCIN/AEI/10.13039/501100011033 and by "ERDF A way of making Europe"; the AGROALNEXT programme supported by MCIN with funding from European Union NextGenerationEU (PRTR-C17.I1) and by Generalitat grant number EUAGROALNEXT/2022/065; and by Generalitat Valenciana grant number CIAPOT/2022/017.

Appendix A. Supplementary data

Supplementary data to this article can be found online at https://doi.org/10.1016/j.micromeso.2024.113314.

References

[1] A. Kumari, M. Zaman, A. Kumar, V.R. Singh, A. Ghosh, S.K. Sahoo, A. Rahaman, S. K. Mandal, S. Bhunia, J. Mater. Eng. Perform. 32 (2023) 10391–10401, https://doi.org/10.1007/s11665-023-07876-8.
[2] R.M. Sábio, A. Bagliotti Meneguin, A. Martins dos Santos, A.S. Monteiro, M. Chorilli, Micropor. Mesopor. Mat. 312 (2021) 110774, 110774.10.1016/j.micromeso.2020.110774.
[3] G.M. Ziarani, R. Moradi, F. Mohajer, A. Badiei, Spectrochim. Acta Mol. Biomol. Spectrosc. 267 (2022) 120580, https://doi.org/10.1016/j.saa.2021.120580.
[4] L. Liao, M. Wang, Z. Li, X. Wang, W. Zhou, Nanomaterials 13 (2023) 468, https://doi.org/10.3390/nano13030468.
[5] J. El Haskouri, D. Ortiz de Zárate, C. Guillem, J. Latorre, M. Caldés, A. Beltrán, D. Beltrán, A.B. Descalzo, G. Rodríguez-López, R. Martínez-Máñez, M.D. Marcos, P. Amorós, Chem. Comm. (2002) 330–331, https://doi.org/10.1039/B110883B.
[6] M. Pérez-Cabero, A.B. Hungría, J.M. Morales, M. Tortajada, D. Ramón, A. Moragues, J. El Haskouri, A. Beltrán, D. Beltrán, P. Amorós, J. Nanopart. Res. 14 (2012) 1045, https://doi.org/10.1007/S11051-012-1045-8.
[7] P. Alfonso Albiñana, J. El Haskouri, M.D. Marcos, F. Estevan, P. Amorós, M.Á. Úbeda, F. Pérez-Pla, J. Catal. 367 (2018) 283–295, https://doi.org/10.1016/j.jcat.2018.09.014.
[8] E. Pellicer-Castell, C. Belenguer-Sapiña, P. Amorós, J. el Haskouri, J.M. Herrero-Martínez, A.R. Mauri-Aucejo, Anal. Chim. Acta 1110 (2020) 26–34, https://doi.org/10.1016/j.aca.2020.03.008.
[9] S. Muñoz-Pina, A. Duch-Calabuig, E. Ruiz de Assín David, J.V. Ros-Lis, P. Amorós, Á. Argüelles, A. Andrés, Food Res. Int. 162 (2022) 112073, https://doi.org/10.1016/j.foodres.2022.112073.
[10] Y. Wan, D. Zhao, Chem. Rev. 107 (2007) 2821–2860, https://doi.org/10.1021/cr068020s.
[11] M.D. Garrido, M. Benítez, J.V. Ros-Lis, P. Amorós, Nano Select (2024) 2300169, https://doi.org/10.1002/nano.202300169.
[12] R. Pujro, P. Crespo, P. Amorós, M. Blanco, S. Cabrera, Rev. Bol. Quim. 24 (2007) 26–32.
[13] C.J. Brinker, Y. Lu, A. Sellinger, H. Fan, Adv. Mater. 11 (1999) 579–585, https://doi.org/10.1002/(SICI)1521-4095(199905)11:7<579::AID-ADMA579>3.0.CO;2-R.
[14] S. Haider, R. Nawaz, M. Anjum, T. Haneef, V.K. Oad, S. Uddinkhan, R. Khan, M. Aquif, Front. Environ. Sci. Eng. 17 (2023) 111, https://doi.org/10.1007/s11783-023-1711-3.
[15] S. Shiva Samhitha, G.M. Raghavendra, C. Quezada, P. Hima Bindu, Mater. Today Proc. 54 (2022) 765–770, https://doi.org/10.1016/j.matpr.2021.11.073.
[16] R. Campos, J. Primera, P. Amorós, L. Huerta, Ciencia 25 (2017) 136–142. ISSN: 1315-2076.
[17] M.M. Trandafir, A. Moragues, P. Amorós, V.I. Parvulescu, Catal. Today 355 (2020) 893–902, https://doi.org/10.1016/j.cattod.2019.02.053.
[18] A. Moragues, F. Neatu, V.I. Paîrvulescu, M.D. Marcos, P. Amorós, V. Michelet, ACS Catal. 5 (2015) 5060–5067, https://doi.org/10.1021/acscatal.5b01207.
[19] C. Rodríguez-Carrillo, J. Torres García, M. Benítez, J. El Haskouri, P. Amorós, J. V. Ros-Lis, Molecules 27 (2022) 2712, https://doi.org/10.3390/molecules27092712.
[20] J. Zhang, D. Zhao, M. Liu, J. Li, Adv. Mater. Res. 557–559 (2012) 1411–1414, https://doi.org/10.4028/www.scientific.net/AMR.557-559.1411.
[21] B. Díaz de Greñu, R. de los Reyes, A.M. Costero, P. Amorós, J.V. Ros-Lis, Nanomater 10 (2020) 1092, https://doi.org/10.3390/nano10061092.
[22] X. Zhou, P.D. Pedrow, Z. Tang, S. Bohnet, S.S. Sablani, J. Tang, Innov. Food Sci. Emerg. Technol. 83 (2023) 103240, https://doi.org/10.1016/j.ifset.2022.103240.
[23] S. Dąbrowska, T. Chudoba, J. Wojnarowicz, W. Łojkowski, Crystals 8 (2018) 379, https://doi.org/10.3390/cryst8100379.
[24] S. Horikoshi, T. Watanabe, A. Narita, Y. Suzuki, N. Serpone, Sci. Rep. 8 (2018) 5151, https://doi.org/10.1038/s41598-018-23465-5.
[25] B. Díaz de Greñu, S. Muñoz-Pina, R. De los Reyes, M. Benítez, J. El Haskouri, P. Amorós, J.V. Ros-Lis, Chem Sus, Chem 16 (2023) e2023001, https://doi.org/10.1002/cssc.202300123.
[26] M. Benítez, C. Rodríguez-Carrillo, S. Sánchez-Artero, J. El Haskouri, P. Amorós, J. V. Ros-Lis, Green Chem. 26 (2023) 785–793, https://doi.org/10.1039/D3GC02875E.
[27] M.D. Garrido, C. García-Llacer, J. El Haskouri, M.D. Marcos, J.F. Sánchez-Royo, A. Beltrán, P. Amorós, J. Coord. Chem. 71 (2018) 776–785, https://doi.org/10.1080/00958972.2018.1442002.
[28] J. Tauc, A. Menth, D.L. Wood, Phys. Rev. Lett. 25 (1970) 749–752, https://doi.org/10.1103/PhysRevLett.25.749.

[29] P.J. Matts, V. Alard, M.W. Brown, L. Ferrero, H. Gers-Barlag, N. Issachar, D. Moyal, R. Wolber, Int. J. Cosmet. Sci. 32 (2010) 35–46, https://doi.org/10.1111/j.1468-2494.2009.00542.x.
[30] Food and Drug Administration, Labeling and effectiveness testing: sunscreen drug products for over-the-counter human use - small entity compliance guide. https://www.fda.gov/media/85172/download/, 2012. (Accessed 11 April 2024).
[31] G. Faraca, C. Vidal-Abarca Garrido, R. Kaps, A. Fernández Carretero, O. Wolf, D. Morera, J. Bastos, M.R. Riera, M. Escamilla, R. Escudero, ISBN 978-92-76-41078-2, https://doi.org/10.2760/195921, JRC126061.
[32] J. El Haskouri, J.M. Morales, D. Ortiz de Zárate, L. Fernández, J. Latorre, C. Guillem, A. Beltrán, D. Beltrán, P. Amorós, Inorg. Chem. 47 (2008) 8267–8277, https://doi.org/10.1021/ic800893a.
[33] J. El Haskouri, D.O. de Zárate, F. Pérez-Pla, A. Cervilla, C. Guillem, J. Latorre, P. Amorós, New J. Chem. 26 (2002) 1093–1095, https://doi.org/10.1039/B205856C.
[34] R.K. Iller, The Chemistry of Silica: Solubility, Polymerization, Colloid and Surface Properties, and Biochemistry, John Wiley & Sons, New York, 1979.
[35] J. Schmidt, W. Vogelsberger, J. Solution Chem. 38 (2009) 1267–1282, https://doi.org/10.1007/s10953-009-9445-9.
[36] D. Ortiz de Zárate, A. Gómez-Moratalla, C. Guillem, A. Beltrán, J. Latorre, D. Beltrán, P. Amorós, Eur. J. Inorg. Chem. 2006 (2006) 2575–2581, https://doi.org/10.1002/ejic.200501140.
[37] M.D. Garrido, N. Puchol, J. El Haskouri, J.F. Sánchez-Royo, J.V. Folgado, V. González Marrachelli, I. Pérez Terol, J.V. Ros-Lis, M.D. Marcos, R. Ruíz, A. Beltrán, J.M. Morales, P. Amorós, Micropor. Mesopor. Mat. 336 (2022) 111863, https://doi.org/10.1016/j.micromeso.2022.111863.
[38] R.S. Dubey, Y.B.R.D. Rajesh, M.A. More, Mater. Today: Proc. (2015) 3575–3579, https://doi.org/10.1016/j.matpr.2015.07.098.
[39] L. Spallino, L. Vaccaro, L. Sciortino, S. Agnello, G. Buscarino, M. Cannas, F. Gelardi, Phys. Chem. Chem. Phys. 16 (2014) 22028–22034, https://doi.org/10.1039/C4CP02995J.
[40] J. El Haskouri, S. Cabrera, M. Gutierrez, A. Beltrán-Porter, D. Beltrán-Porter, M. D. Marcos, P. Amorós, Chem. Comm. 4 (2021) (2001) 309–310, https://doi.org/10.1039/B008810M.
[41] M. Itoh, H. Hattori, K. Tanabe, J. Catal. 35 (1974) 225–231, https://doi.org/10.1016/0021-9517(74)90201-2.
[42] A. Sayari, Chem. Mater. 8 (1996) 1840–1852, https://doi.org/10.1021/cm950585+.
[43] G. Petrini, A. Cesana, G. De Alberti, F. Genoni, G. Leofanti, M. Padovan, G. Paparatto, P. Rofia, Stud. Surf. Sci. Catal. 68 (1991) 761–766, https://doi.org/10.1016/S0167-2991(08)62710-X.
[44] M. Anpo, H. Nakaya, S. Kodama, Y. Kubokawa, J. Phys. Chem. 90 (1986) 1633–1636.
[45] B. Erdem, R.A. Hunsicker, G.W. Simmons, E.D. Sudol, V.L. Dimonie, M.S. El-Aasser, Lagmuir 17 (2001) 2664–2669, https://doi.org/10.1021/la0015213.
[46] M.W. Gaultois, A.P. Grosvenor, J. Mater. Chem. 21 (2011) 1829–1836, https://doi.org/10.1039/C0JM03464A.
[47] U. Arellano, J.A. Wang, L.F. Chen, M. Asomoza, A. Guzmán, S. Solís, A. Estrella, S. Cipagauta, L.E. Noreña, Catal. Today 349 (2020) 128–140, https://doi.org/10.1016/j.cattod.2018.05.017.
[48] F. Esin Yakin, M. Barisik, T. Sen, J. Phys. Chem. C 124 (2020) 19579–19587, https://doi.org/10.1021/acs.jpcc.0c04602.
[49] M. Itoh, H. Hattori, K. Tanabe, J. Catal. 35 (1974) 225–231, https://doi.org/10.1016/0021-9517(74)90201-2.
[50] R. Ghamarpoor, A. Fallah, M. Jamshidi, Sci. Rep. 12 (2023) 9793, https://doi.org/10.1038/s41598-023-37057-5.
[51] S. Ura, T. Nakashiba, T. Suhara, H. Nishihara, P.V. Lambeck, Jpn. J. Appl. Phys. 39 (2000) 1487–1489, https://doi.org/10.1143/JJAP.39.1487.
[52] C.C. Li, Y.T. Chen, Y.T. Lin, S.F. Sie, Y.W. Chen-Yang, Colloids Surf. B Biointerfaces 115 (2014) 191–196, https://doi.org/10.1016/j.colsurfb.2013.11.011.
[53] Y.W. Chen-Yang, Y.T. Chen, C.C. Li, H.C. Yu, Y.C. Chuang, J.H. Su, Y.T. Lin, Mater. Lett. 65 (2011) 1060–1062, https://doi.org/10.1016/j.matlet.2010.12.034.
[54] J.S. Barbosa, D.M.A. Neto, R.M. Freire, J.S. Rocha, L.M.U.D. Fechine, J. C. Denardin, A. Valentini, T.G. de Araújo, S.E. Mazzetto, P.B.A. Fechine, Ultrason. Sonochem. 48 (2018) 340–348, https://doi.org/10.1016/j.ultsonch.2018.06.015.
[55] P. da Silva Marcelino, R. Miliani Martinez, A.L. Máximo Daneluti, A.L. Morocho-Jácome, F.V. Lima Solino Pessoa, P. Rijo, C. Rosado, M.V. Robles Velasco, A. Rolim Baby, Cosmetics 10 (2023) 46, https://doi.org/10.3390/cosmetics10020046.
[56] Department of Health and Human Services. Food and Drug Administration. 21 CFR Parts 201, 310, 347 and 352 [Docket No. 1978N-0038] (formerly Docket No. 78N-0038) RIN 0910-AF43, 84 (2019) 6204-6275.